J Mater Sci: Mater Electron (2018) 29:1914–1924
DOI 10.1007/s10854-017-8101-1

Enhanced photoluminescence of $CoWO_4$ in $CoWO_4/PbWO_4$ nanocomposites

M. Jeyakanthan[1] · Uma Subramanian[1] · R. B. Tangsali[1]

Received: 2 August 2017 / Accepted: 19 October 2017 / Published online: 25 October 2017

Abstract $CoWO_4/PbWO_4$ nanocomposites were successfully synthesized at room temperature (RT) by co-precipitation route without using any templates or surfactants and sintered at 600 °C for good crystallization. The sintered samples were characterized by X-ray diffraction, Fourier transform infrared spectroscopy, scanning electron microscopy (SEM), transmission electron microscopy and Zeta potential measurements. UV–Visible diffuse reflectance spectroscopy, photoluminescence (PL) and PL lifetime were studied at RT. The results indicate that the composites have two-phase composition: $CoWO_4$ and $PbWO_4$. SEM micrograph and zeta potential measurements reveal particle agglomeration. The intrinsic PL peak emission at 467 nm of $CoWO_4$ nano sample was enhanced upto four times by optimizing the atomic ratio of Pb/Co concentration. The interconnected interface of $CoWO_4/PbWO_4$ nanocomposites could have led to increase in number of recombination of electron hole pairs in $CoWO_4$ and enhanced its intrinsic PL emission intensity. The mechanism of enhanced PL emission for the $CoWO_4/PbWO_4$ nanocomposites can be attributed to charge transfer between $[WO_4]^{2-}$ and $[WO_6]^{6-}$ complexes due to intra particle agglomeration leading to possible interface.

Electronic supplementary material The online version of this article (doi:10.1007/s10854-017-8101-1) contains supplementary material, which is available to authorized users.

✉ Uma Subramanian
us00@yahoo.com

[1] Department of Physics, Goa University, Taleigao Plateau, Goa 403206, India

1 Introduction

Nanocomposites have been studied extensively for enhancing the unique properties of metal oxide semiconductors [1]. Preparation of nanocomposites by wet chemical methods is used to make nanostructured materials with variable optical and electronic properties for the development of new multifunctional materials. In nanocomposites with type I band alignment the band gap of one material completely overlaps the band gap of other adjacent material. If the materials with appropriate band offsets are chosen to form the nanocomposites to trap electron–hole pairs in specific regions of the material then increase in recombinations leading to enhanced luminescent emission intensities occur [2]. For example, De Santana et al. reported the enhancement of the PL intensity of silver tungstate and silver molybdate nanocomposites [3]. Jian Ming Lin et al. reported the enhanced PL emission of ZnO nanorods in SnO/ZnO nanocomposites [4]. The enhanced photocatalytic and photoluminesce of ZnO–$ZnWO_4$ nanocomposites has been reported by Jiang et al. [5]. In nanocomposites with type II alignment of band gaps, the band edges of one domain lie lower in energy than the band edges of the other adjacent material, inducing spatial separation of electron–hole pairs (excitons) between different parts of the composite nanostructure, which can be used for the development of photovoltaic and photocatalytic materials [2]. Guo et al. reported that $CaWO_4/Bi_2WO_6$ enhance the photocatalytic activity of Bi_2WO_6 [6]. The composite of $Bi_2WO_6/ZnWO_4$ enhance the photocatalytic activity of $ZnWO_4$ due to effective separation of photoinduced electron hole pairs and the low recombination rate of charge carriers [7].

Metal tungstates are important class of self-activated luminescent materials due to their broad applications as phosphors, laser materials, and scintillation detectors

[8]. They crystallize into two structures based on their cationic radii, i.e., wolframite (rA < 0.77 Å) and scheelite (rA > 0.90 Å) [9, 10]. In scheelite and wolframite structured tungstates the intrinsic luminescence arise due to annihilation of self-trapped exciton (STE), which forms excited $[WO_4]^{2-}$ or $[WO_6]^{6-}$ complexes respectively [11]. Some of the divalent transition metal tungstates have also gained commercial interest in lasers and fluorescent lamps [12]. In addition, these materials also find applications as catalysts and humidity sensors [13].

$CoWO_4$ is a wolframite structured p-type semiconductor. Very few works has been done in enhancing the PL of $CoWO_4$ nanocrystals. Ce^{3+} doping in $CoWO_4$ nanomaterial doubled the PL emission intensity as compared to that of undoped $CoWO_4$ due to the formation of Ce_2WO_6 interface [14] also PL intensity of bulk material sintered at 1000 °C was found to be 40 times less than that of the nanomaterial sintered at 600 °C. Upconversion luminescence of Ce^{3+} doped $CoWO_4$ reported by Subramanian et al. [15]. Yb doping in $CoWO_4$ nanoparticles quench the intrinsic emission [16]. $CoWO_4$ nanowire exhibits IR emission at the ambient temperature under UV excitation [17]. Instead of using single phase material coupling with other semiconductor has also been found to be an effective means to enhance the luminescence properties of oxide nanomaterials [18, 19]. PL lifetime measurements have been reported for some wolframite structured tungstates other than $CoWO_4$ [20–22]. $PbWO_4$ is a scheelite structured wide band semiconductor. PL properties of $PbWO_4$ have been widely studied [23–25].

To the best of our knowledge PL study of $CoWO_4/PbWO_4$ nanocomposites which form type I band alignment have not been reported. We have previously published the outline of our initial work on the PL of Pb^{2+} doped $CoWO_4$ nanocrystalline materials in the conference proceedings [26]. In this paper we have reported elaborative work on $CoWO_4/PbWO_4$ nanocomposites by optimizing the atomic ratio of Pb/Co for maximum PL emission, explained the mechanism for enhancement of PL emission intensity in detail with more supporting measurements, reported PL lifetime results. We prepared the samples by simultaneous precipitation of both the ($CoWO_4$ and $PbWO_4$) nano compounds because $CoWO_4$ crystallizes into wolframite monoclinic structure and $PbWO_4$ crystallizes into scheelite tetragonal structure. Also the ionic radius of Co^{2+} (0.65 Å) is much smaller than that of Pb^{2+} (1.19 Å). In wolframite $CoWO_4$ structure, Co is coordinated with six oxygen atoms and W also is coordinated with six oxygen atoms. In scheelite $PbWO_4$ structure, Pb is coordinated with eight oxygen atoms and W is surrounded by four oxygen atoms so there is less chance to Pb getting into $CoWO_4$ lattice and Co into $PbWO_4$ lattice in simple coprecipitation method. The $CoWO_4/PbWO_4$ nanocomposites were sintered at 600 °C for good crystallization and characterized by XRD, TEM, SEM, FTIR and EDS methods. Room temperature optical absorption and characteristic PL intensities of $CoWO_4$ nanocrystalline materials were found to be enhanced for $CoWO_4/PbWO_4$ nanocomposites. In the present work maximum intrinsic PL emission which is four times than the $CoWO_4$ is achieved by introducing and optimizing the additional absorbing $(WO_4)^{2-}$ complexes through $PbWO_4$. Also particle size, bandgap energy and PL lifetime are controlled by the ratio of Pb/Co atomic concentration. Reasons for enhancement of PL emission intensity of $CoWO_4/PbWO_4$ nanocomposites are discussed in detail. Agglomeration due to optimised ratio of Pb/Co (0.028) is found to be advantageous in enhancing the intrinsic luminescence of $CoWO_4$ nanomaterials.

2 Experimental section

2.1 Materials

Analytical grade cobalt nitrate $Co(NO_3)_3{\cdot}6H_2O$, sodium tungstate $Na_2WO_4{\cdot}2H_2O$ and lead nitrate $Pb(NO_3)_2$ were used for sample preparation.

2.2 Sample preparation

$CoWO_4$ and $PbWO_4/CoWO_4$ nanocomposite samples were prepared at room temperature by co-precipitation method [14]. $Co(NO_3)_2{\cdot}6H_2O$, $Pb(NO_3)_2$ and $Na_2WO_4{\cdot}2H_2O$ were separately dissolved in distilled water to make aqueous solutions. The nitrate aqueous solutions were mixed and stirred for 10 min. $Na_2WO_4{\cdot}2H_2O$ aqueous solution was slowly added to the mixed nitrate solution with constant stirring for 3 h and the purple color precipitate was filtered out. Then the precursor was washed several time with distilled water, dried at 100 °C, sintered at 600 °C for 1 h and were labeled according to increase in Pb/Co atomic ratio 0, 0.01, 0.015, 0.028, 0.036 and as S0, S1, S2, S3 and S4.

2.3 Characterization

The XRD patterns of the samples were recorded by Rigaku X-ray diffractometer with Cu-K_α radiation. UV–Vis diffused reflectance spectra (DRS) were recorded using SHIMADZU UV-2401PC Spectrophotometer. The morphologies of synthesized samples were analyzed by EVO-18 Carls-Zeiss scanning electron microscope and Hitachi H-600 TEM. Zeta potential value of the samples is measured by Zetasizer Nano Z Malvern instruments. Vibrational frequencies of samples were recorded using SHIMADZU IR-800 Spectrometer. Elemental compositions of the samples were obtained by analyzing EDS recorded with JEOL-JSM 5800 LV scanning electron microscope. PL spectra and PL lifetime were recorded using PTI Spectrofluorometer QM-40 with 150 W

Xenon steady source lamp and 150 W Xenon pulsed source lamp respectively.

3 Results and discussion

3.1 X-ray diffraction analyses

Powder XRD patterns of $CoWO_4$ and $CoWO_4/PbWO_4$ composites sintered at 600 °C are shown in Fig. 1. XRD patterns reveal that the sample S0 ($CoWO_4$) shows single phase formation having wolframite monoclinic structure and space group P2/c matching with JCPDS: 072-0479 [14] and all the composite samples showed wolframite monoclinic phase of $CoWO_4$ and $PbWO_4$ phase which coincide with the reported data of scheelite type tetragonal structure with space group I41/a [JCPDS: 08-0476] [27].

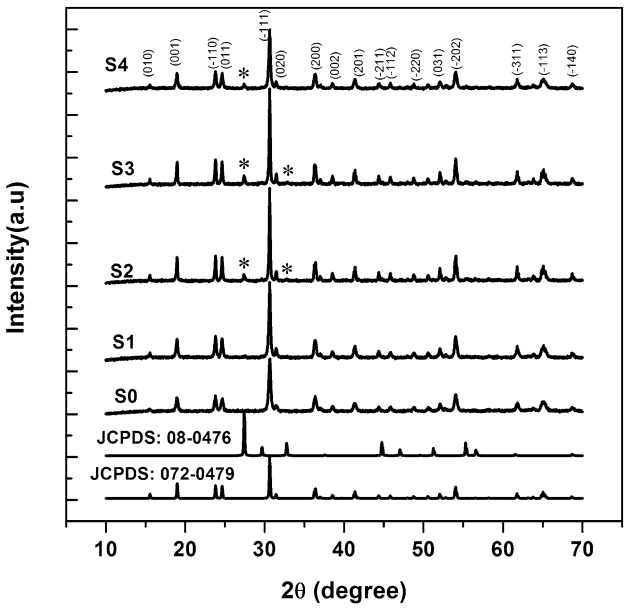

Fig. 1 XRD patterns of S0, S1, S2, S3, S4 and samples and '*' denotes $PbWO_4$ phase

The emergence of additional peaks located at 27.6°, 32.8° (major peak (121) plane at 27.6° is marked by '*') in the XRD patterns confirm the $PbWO_4$ phase in the composite samples. Scherrer formula and Williamson–Hall equation [28] used to estimate average crystallite sizes for the prominent $CoWO_4$ peaks (001, −110, 011, −111, 200, 201, −202, −311 and 113) are given as:

$$D = \frac{K\lambda}{\beta \cos\theta} \tag{1}$$

$$\beta_{hkl} \cos\theta = \frac{K\lambda}{D} + 4\varepsilon \, sin\theta \tag{2}$$

where D is average crystallite size, K is a constant 0.89, λ is the X-ray wavelength (0.15418 nm), θ is the Bragg angle, β is the FWHM of the XRD peak in radians and ε is the lattice strain.

Figure 2a shows the average crystallite size (calculated by Scherrer formula) variation of samples with increase in Pb/Co atomic ratio. Initially the crystallite sizes increase with increase in Pb/Co atomic ratio and then decrease with further increase in Pb/Co atomic ratio. Larger crystallite sizes are observed for samples S2 and S3. Figure 2b shows variation of lattice strain (calculated using Williamson–Hall plots) with increasing Pb/Co atomic ratio. The lattice strain is minimum for S2 and S3 samples. Calculation of lattice parameter values for both the phases were done using Rietveld profile fitting method shown in Fig. 3 and are given in Tables 1 and 2. These values are matched with standard

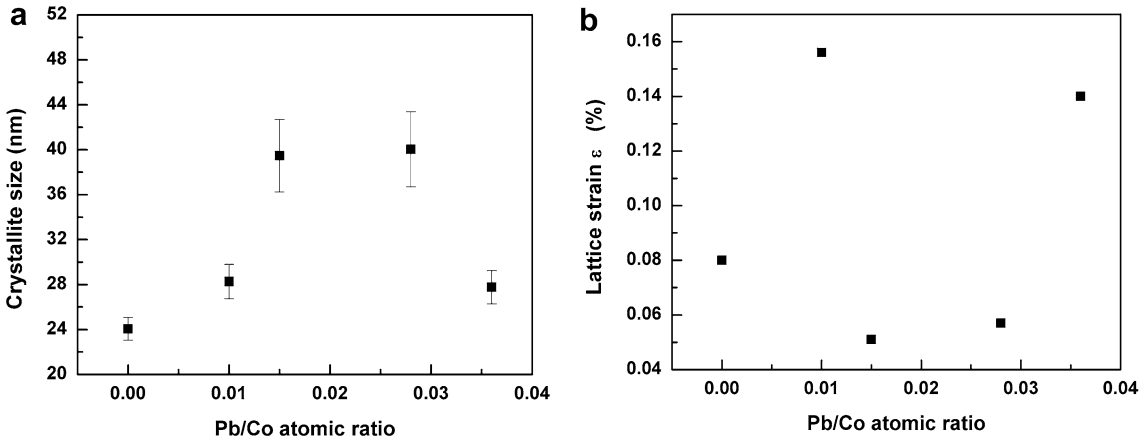

Fig. 2 **a** Crystallite size calculated by Scherrer formula versus Pb/Co atomic ratio. **b** Lattice strain versus Pb/Co atomic ratio of $CoWO_4$ and $CoWO_4/PbWO_4$ composites

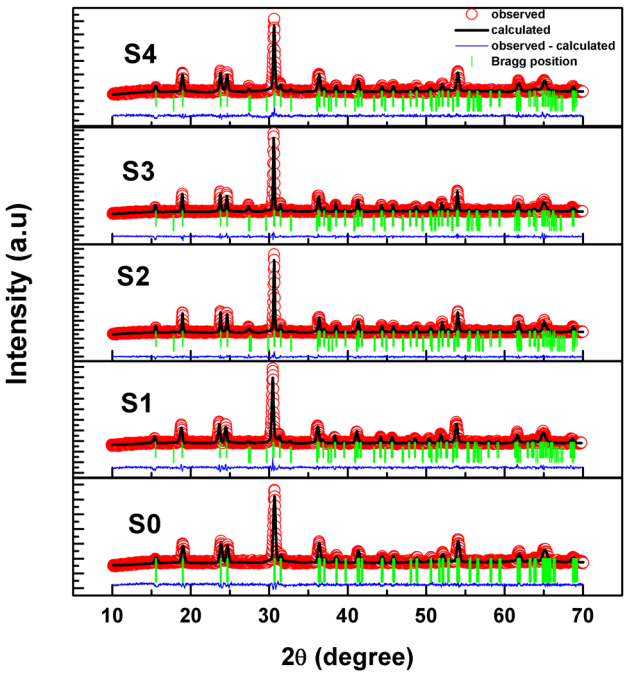

Fig. 3 Rietveld refinement patterns of $CoWO_4$ and $CoWO_4/PbWO_4$ composite samples

value of JCPDS: 072-0479 and JCPDS: 08-0476 for $CoWO_4$ and $PbWO_4$ respectively.

3.2 SEM and EDAX analyses

The SEM images of $CoWO_4$ and $CoWO_4/PbWO_4$ are shown in Fig. 4a–e. The sample S0 has some clusters. When $PbWO_4$ phase mixing is done for S1, particles involving $PbWO_4$ and $CoWO_4$ start agglomerating. As the atomic ratio of Pb/Co are increased for sample S2 more agglomerations and merging of particles involving $CoWO_4$ and $PbWO_4$ occur. Further increase in atomic ratio of Pb/Co in sample S3 leads to maximum agglomeration. When atomic ratio of Pb/Co concentration is still increased in sample S4, agglomeration decreased considerably due to the starting of separation of particles of $PbWO_4$ and $CoWO_4$. Nano-powder is prone to soft reunion due to its small particles and has a great specific surface. Surface atoms of powder are extremely active for the presence of large number of vacancy bonds and make the van der Waals force which is quite large. The presence of van der Waals force is easy to cause the particle agglomeration [29]. Researchers found that the zeta potential causes particle dispersion [30]. Zeta potential values measured for the samples are given in Table 3. Lower zeta potential values for samples S2 and S3 confirm larger agglomerations. Enrichment of $PbWO_4$ particle in the powder surface is able to increase the surface potential of the powder and repulsive effects between the same kinds of particles. Thereby the action of the van der Waals force is offset and agglomeration of the powder is reduced for S4 sample. These results are also supported by the variation of crystallite size and lattice strain with increase in molar ratio of Pb/Co as shown in Fig. 2a, b respectively.

TEM micrograph was observed for S0 sample as shown in Fig. 4f. The average particle size of the material as observed from TEM micrograph is 50.8 nm with a standard deviation of ±9.3 nm for an ensemble size of 21 particles and that calculated from XRD pattern using Scherrer formula is 24 nm.

EDS of samples are shown in Fig. 5a–e. These indicate that all the elements were present in the appropriate amount without any impurities. Concentration of the added Pb/Co atomic ratio was calculated from these spectra.

3.3 FTIR analyses

The FTIR spectra of the synthesized samples are shown in Fig. 6. The stretching absorption bands appearing in the low frequency region of 400–1000 cm^{-1} belong to the characteristic deformation modes W–O, and W–O–W bridges. IR spectra below 500 cm^{-1} could be due to the deformation modes of W–O bonds in $[WO_6]^{6-}$ octahedra or the deformation of W–O–W bridges. The bands positioned at 623, 601 and 824 cm^{-1} are associated with the O–W–O vibration

Table 2 Lattice constants in tetragonal phase of $PbWO_4$ in $CoWO_4/PbWO_4$ nanocomposites

Sample	a = b (Å)	c (Å)	α = γ = β(°)
S1	5.47294 ± 0.00082	12.03815 ± 0.00154	90.00000
S2	5.43818 ± 0.01389	11.77181 ± 0.06142	90.00000
S3	5.46224 ± 0.00089	12.05696 ± 0.00502	90.00000
S4	5.46160 ± 0.00097	12.04600 ± 0.00565	90.00000

Table 1 Lattice constants in monoclinic phase of $CoWO_4$ in $CoWO_4/PbWO_4$ nanocomposites

Sample	a (Å)	b (Å)	c (Å)	α = γ(°)	β(°)
S0	4.66588 ± 0.00070	5.67840 ± 0.00077	4.94847 ± 0.00070	90.00	90.11813 ± 0.01468
S1	4.68930 ± 0.00000	5.70475 ± 0.00000	4.96916 ± 0.00000	90.00	90.10091 ± 0.00000
S2	4.67298 ± 0.00000	5.68778 ± 0.00000	4.95248 ± 0.00000	90.00	90.04226 ± 0.00000
S3	4.66046 ± 0.00000	5.67390 ± 0.00000	4.93972 ± 0.00000	90.00	90.08661 ± 0.00000
S4	4.67398 ± 0.00000	5.68551 ± 0.00000	4.95396 ± 0.00000	90.00	90.12841 ± 0.00000

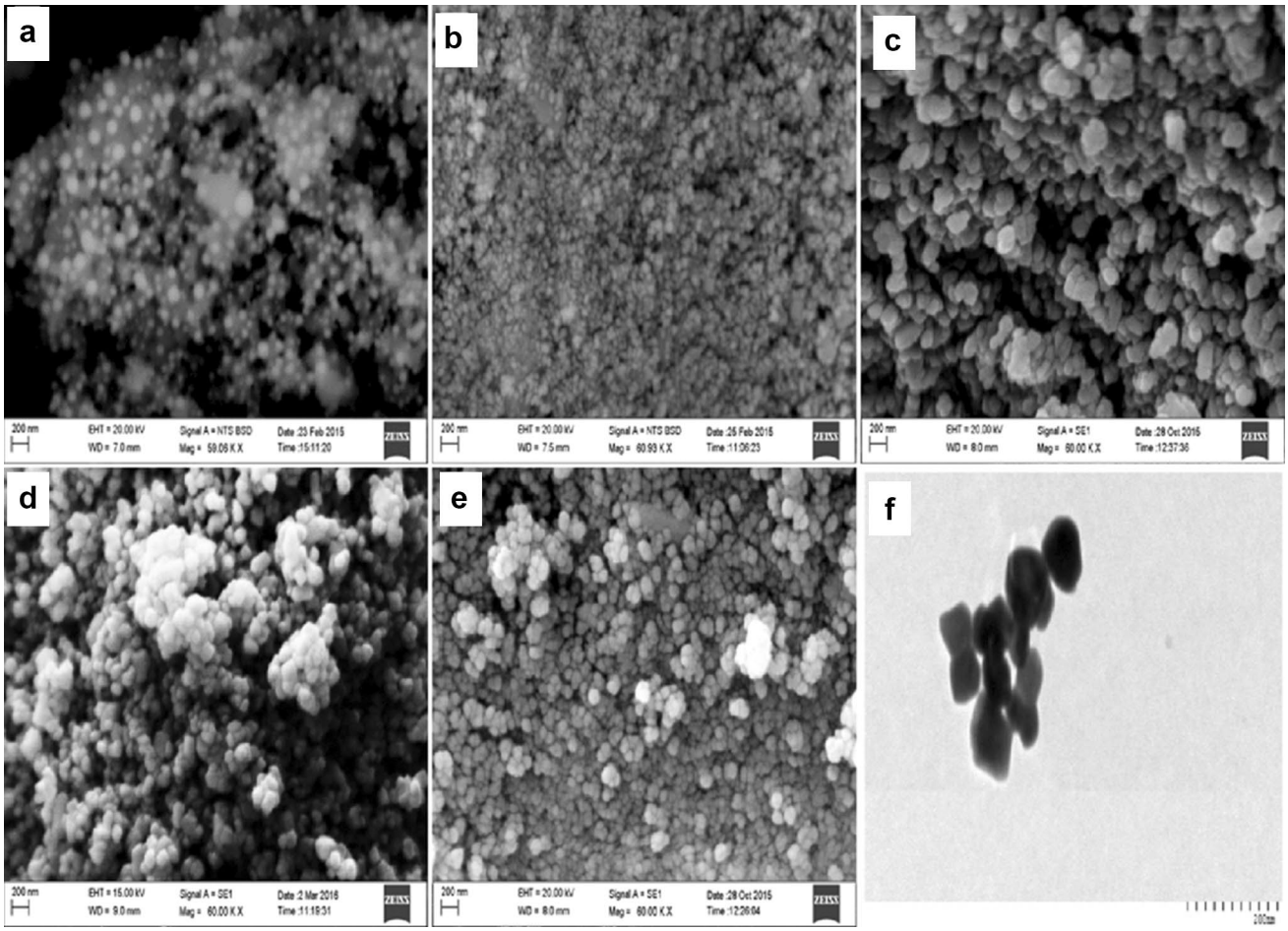

Fig. 4 SEM pictures of **a** S0, **b** S1, **c** S2, **d** S3, **e** S4 samples, **f** TEM image of S0 sample

Table 3 Zeta potential values of $CoWO_4$ and $CoWO_4/PbWO_4$ samples

Sample	Zeta potential (mV)
S0	− 10.38
S1	− 3.66
S2	− 2.85
S3	− 1.03
S4	+ 12.3

mode and the W–O bond stretching, respectively [31]. The bands at 864 and 690 cm^{-1} are attributed to the stretching vibration of W–O–W bridging bonds. The peak appearing at 528 cm^{-1} is due to the asymmetric stretching vibration of the $(WO_6)^{6-}$ group and the stretching mode for W–W bonds. The sharp peak at 465 cm^{-1} is attributed to the bending mode of $(WO_6)^{6-}$ groups.

3.4 Optical absorption study

Figure 7 shows diffuse reflectance spectra of the nanocomposites samples. They exhibit absorption band in the range of 220–475 nm and a broad peak around 586 nm with a small shoulder around 525 nm. The absorption intensities of the band between 200 and 475 nm are almost double than that of the broad peak around 586 nm for all the samples. Absorption band in the range of 200–475 nm are due to the excitation of electrons from oxygen O_{2p} orbital to tungsten W_{5d} orbital in the $[WO_4]^{2-}$ and $[WO_6]^{6-}$ groups due to ultraviolet energy absorption. In the excited state of $[WO_6]^{6-}$ and $[WO_4]^{2-}$ groups, the hole (on the oxygen) and the electron (on the tungsten) forms an exciton because of their strong interactions [10]. The peak absorption observed around 586 nm is due to the d–d transitions from $^4A_2 \rightarrow {}^4T_{1(P)}$ levels of the Co^{2+} ions [14].

Tauc plot of absorption spectra for calculating bandgap energies of the samples are shown in Fig. 8a and values are tabulated in Table 4. Plot of bandgap energies versus Pb/Co atomic ratio is given in Fig. 8b. Variation of bandgap energy is from 2.856 ± 0.003 to 2.900 ± 0.003 eV. Samples with higher particle size, i.e., S2 and S3 have slightly larger bandgap energies as compared to other samples. Generally, the band gap energies shifted to higher

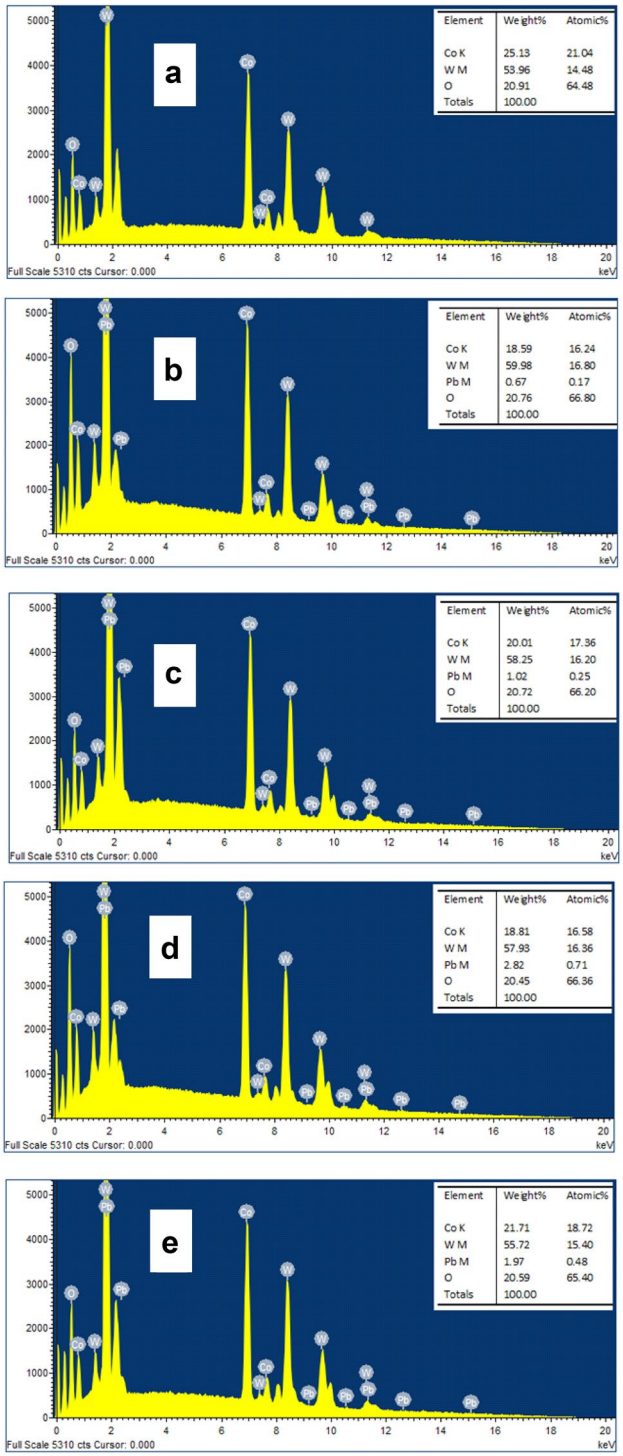

Fig. 5 EDS spectra of **a** S0, **b** S1, **c** S2, **d** S3, **e** S4 samples

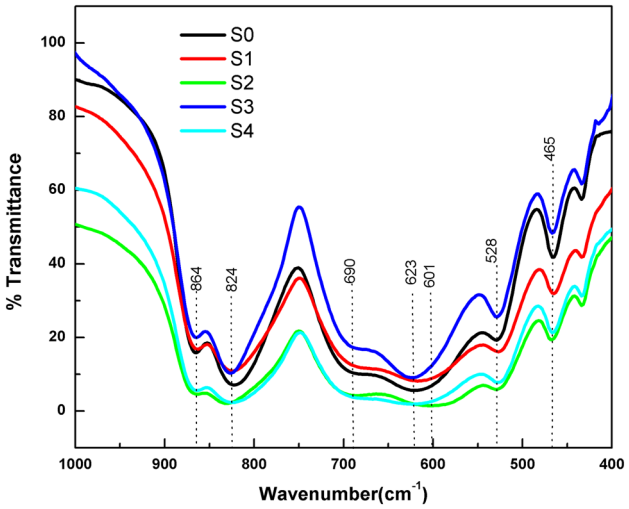

Fig. 6 FTIR spectra of S0, S1, S2, S3, S4 samples

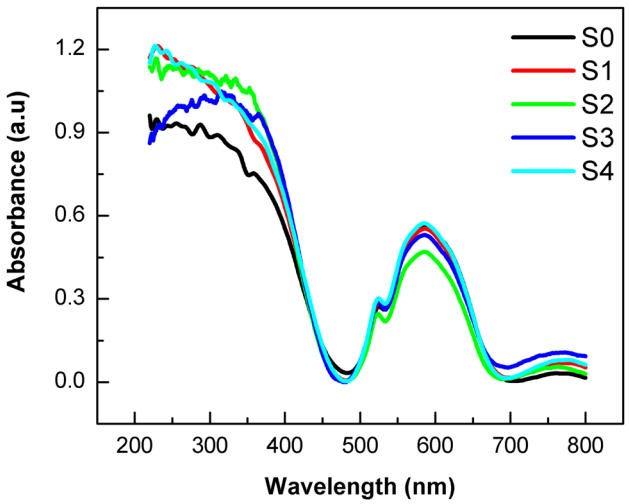

Fig. 7 UV–Visible spectra of $CoWO_4$ and $CoWO_4/PbWO_4$ nanocomposites

energy due to particle size reduction which is explained by quantum confinement effect [32] which is valid only for particle sizes < 10 nm. The band gap energies of the present nanocomposite decreased for smaller particle size samples which are similar to that observed in many oxide nanocrystals [33]. From the viewpoint of solid-state physics, energy bands are formed from overlapping orbital states. As the neighboring atoms are apart from each other within a solid, the basic functions and orbits overlap more weakly, producing decreased dispersion of the electron bands in k space and consequently decreased bandwidths along the energy axis [34]. In other words, the bandwidth will decrease with the reduction of overlap [35]. Therefore increase in the bandgap energies for more agglomerated samples are due to orbital overlapping of $CoWO_4$ and $PbWO_4$ complexes.

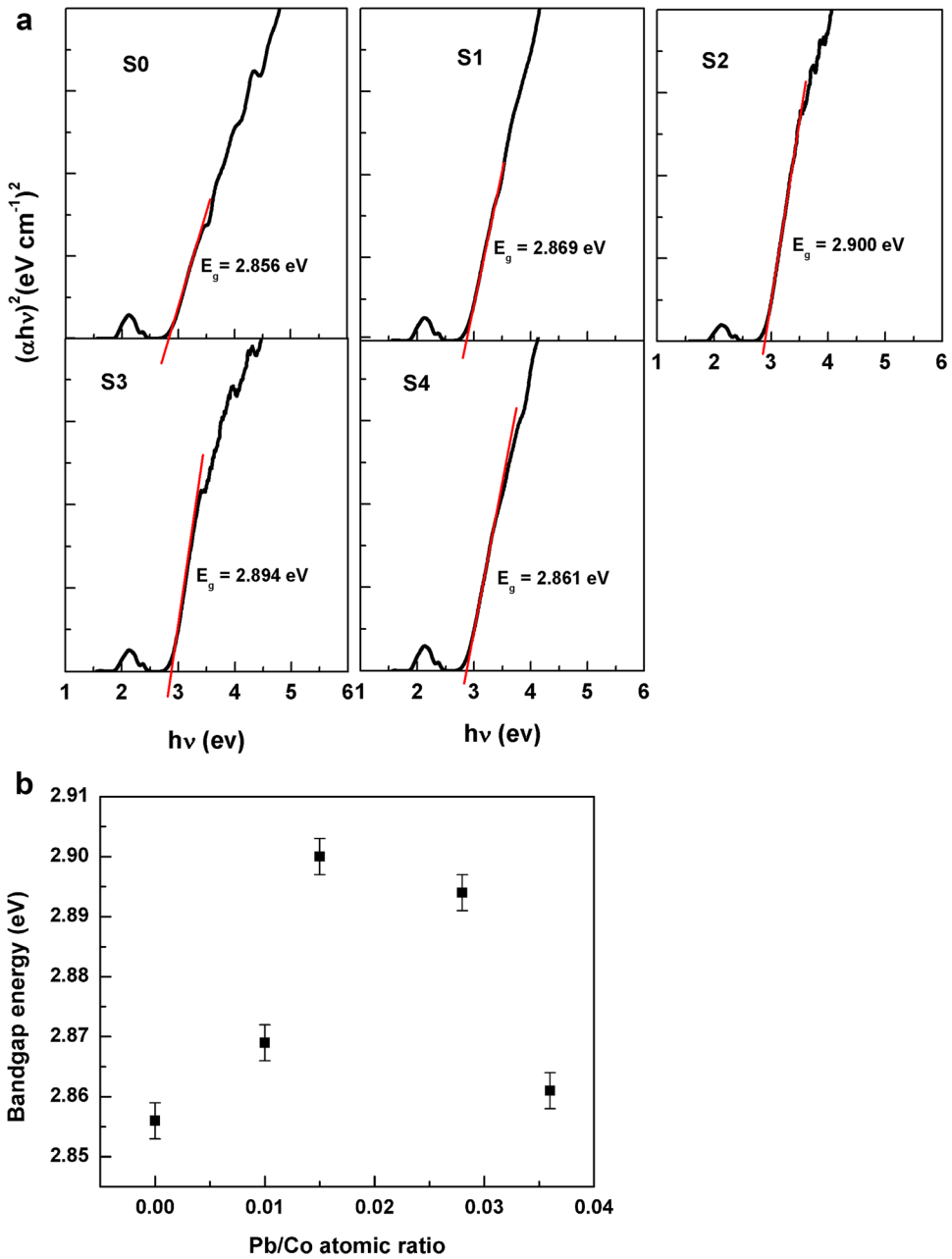

Fig. 8 **a** Tauc plot of $CoWO_4$ and $CoWO_4/PbWO_4$ nanocomposites. **b** Bandgap energy versus Pb/Co atomic ratio

Table 4 Bandgap energy of the samples

Sample	Bandgap energy (eV)
S0	2.856 ± 0.003
S1	2.869 ± 0.003
S2	2.900 ± 0.003
S3	2.894 ± 0.003
S4	2.861 ± 0.003

3.5 Photoluminescence (PL) study

Room temperature PL spectra of the samples with 210 nm excitation wavelength are shown in Fig. 9. The spectra exhibiting broad bluish-green emissions centered at 467 nm and shoulder around 536 nm are intrinsic luminescence of $CoWO_4$ caused by the annihilation of self-trapped excitons, which form excited $[WO_6]^{6-}$ complexes. The $CoWO_4/PbWO_4$ composite changed the PL emission intensities of $CoWO_4$ but did not alter the structure of spectrum. The 467 nm PL intensity is maximum for S3 sample as shown in inset of Fig. 9 and is four times higher than the $CoWO_4$ sample PL intensity. In scheelite and wolframite structured tungstates the intrinsic luminescence arises due to annihilation of self-trapped exciton (STE), which forms excited $[WO_4]^{2-}$ or $[WO_6]^{6-}$ complexes respectively [11]. Maximum agglomerations and merging of particles involving $CoWO_4$

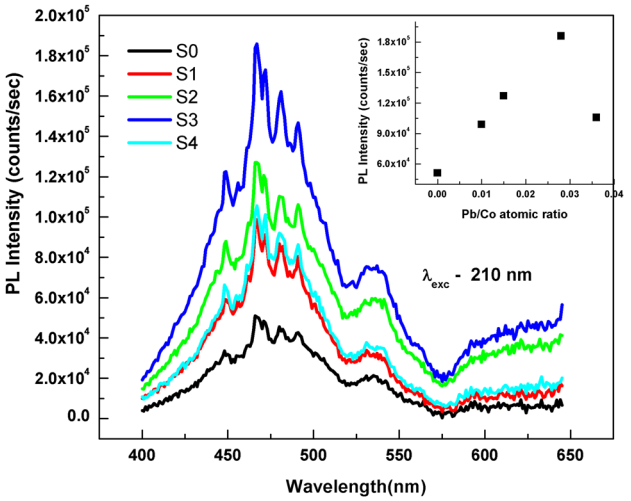

Fig. 9 PL spectra of $CoWO_4$ and $CoWO_4$/$PbWO_4$ nanocomposites excited with 210 nm. Inset shows the variation of PL peak intensity with Pb/Co atomic ratio

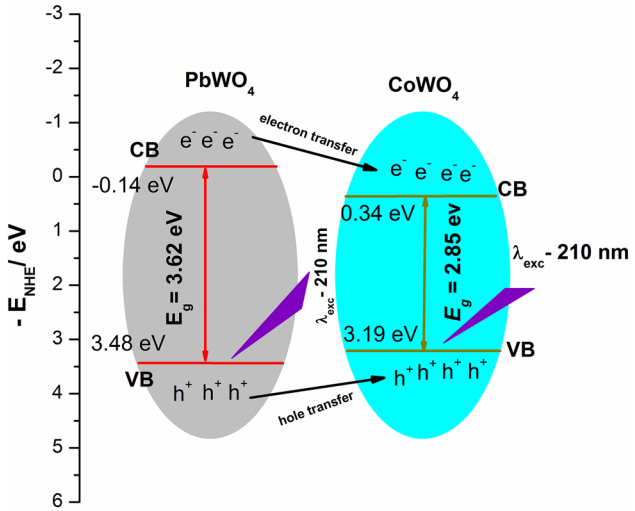

Fig. 10 Band structure diagram and charge transfer processes in $CoWO_4$/$PbWO_4$ nanocomposites

(wolframite structured) and $PbWO_4$ (scheelite structured) are there for S3 sample.

The cluster-to-cluster charge-transfer (CCCT) in a crystal, containing more than one kind of cluster, is characterized by excitations involving electronic transitions from one cluster to another. Longo et al. demonstrated that the CCCT mechanism in hierarchical assemblies of $CaMoO_4$ ($[MoO_4]^x$–$[MoO_3.V^z_O]$ or $[CaO_8]^x$–$[CaO_7.V^z_O]$) and ($[MoO_4]$'–$[MoO_3.V_O]$ or $[CaO_8]^0$–$[CaO_7.V_O]$) can be considered a new class of electronic transitions involved during the PL emissions [36]. In this work we consider the charge transfer mechanism from the excited $[WO_4]^{2-}$ clusters of $PbWO_4$ to $[WO_6]^{6-}$ clusters of $CoWO_4$ to be responsible for the enhanced PL intensity of the more agglomerated samples S2 and S3. Band structure diagram and charge transfer processes in $CoWO_4$/$PbWO_4$ nanocomposites are represented in Fig. 10. The conduct band (CB) and valence band (VB) potentials of the samples at the point of zero charge are calculated by the following equation [37] by using the bandgap values estimated by us.

$$E_{VB} = X - Ee + 0.5Eg \tag{3}$$

$$E_g = E_{VB} - E_g \tag{4}$$

where X is the absolute electronegativity of the semiconductors, which is defined as the geometric average of the absolute electronegativity of the constituent atoms, E_e is the energy of free electrons on the hydrogen scale (4.5 eV), and E_g is the bandgap. For $CoWO_4$, the X is calculated to be 6.22 eV, consequently. The band gap values of the $CoWO_4$ and $PbWO_4$ is 2.85 and 3.62 eV respectively. The band gap calculation of $PbWO_4$ is given in the supporting information SI1. The E_{CB} and E_{VB} values of $CoWO_4$ are estimated to be 0.29 and 3.14 eV, respectively. The X of $PbWO_4$ is calculated to be 6.13 eV, and the E_{CB} and E_{VB} are estimated to be − 0.18 and 3.44 eV respectively. Under 210 nm UV irradiation, $PbWO_4$ and $CoWO_4$ would be excited simultaneously and generate electron hole pairs. The CB-electrons from the excited $[WO_4]^{2-}$ clusters of $PbWO_4$ would easily flow into the CB edge of $[WO_6]^{6-}$ clusters of $CoWO_4$ through the interface because the CB edge of $PbWO_4$ is higher than that of $CoWO_4$. Also the VB edge level of $PbWO_4$ is lower than that of $CoWO_4$ and holes in the VB edge of $PbWO_4$ will transfer to that of $CoWO_4$ by the control of the interface due to agglomeration leading to more recombination and enhancement of emissions from the $[WO_6]^{6-}$ complexes of $CoWO_4$. Similar results were reported earlier for ZnO/SnO naocomposites [6].

Schematic energy level diagrams on the basis of previously reported literature [17] for the $[WO_6]^{6-}$ complex, excitation and emissions are shown in Fig. 11. The transition in $[WO_6]^{6-}$ complexes from two close $_3T^{1u}$ levels to the $_1A^{1g}$ level are responsible for the 467 nm emission. The spin-forbidden transitions from T^{1g} to $_1A^{1g}$ are partly allowed by spin–orbit coupling, and this would contribute to the luminescence on the longer wavelength of 530 nm [17]. In agglomerated samples the orbitals of $CoWO_4$ and $PbWO_4$ complexes are overlapped which favours the transfer of charge from WO_4^{2-} to WO_6^{6-} complexes. Also when the particle size is large due to agglomeration, the surface grain boundaries are less and charge transfer between $[WO_4]^{2-}$ complexes $[WO_6]^{6-}$ complexes increase.

Figure 12 shows PL decay kinetics of 467 nm emission with 210 nm excitation measured at RT. The decay curves were well fitted with single exponential function:

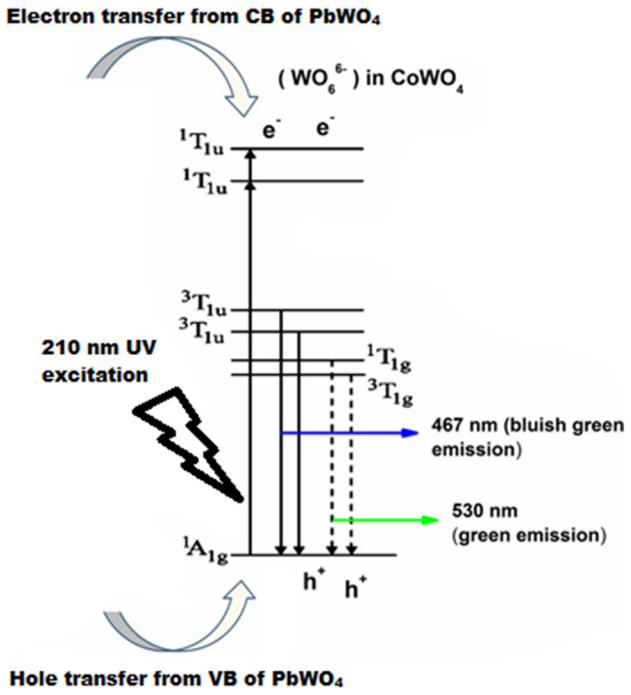

Fig. 11 Emission processes from $(WO_6)^{6-}$ complexes of $CoWO_4$ in $CoWO_4/PbWO_4$ nanocomposites

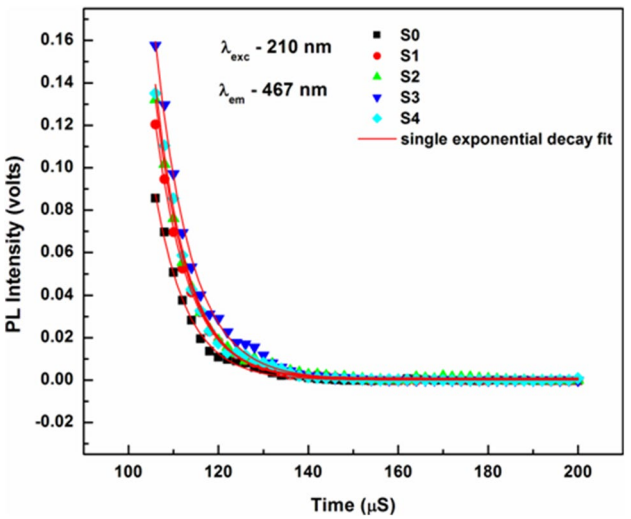

Fig. 12 PL decay curves of the samples

$$I = A\exp(-t/\tau) + I_0 \quad (5)$$

where I_0 and I are the initial and instantaneous luminescence intensities respectively, A is a constant and t is the measurement time. The τ represents the lifetime of the PL emission. The calculated values of τ are tabulated in Table 5. It is observed that PL lifetime of highly agglomerated samples S2 and S3 are little (< 10%) longer than that of the other samples S0, S1, S4. We believe that, in highly agglomerated samples S2 and S3 the cluster to cluster charge transfer (CCCT) process from WO_4^{2-} to WO_6^{6-} complexes enhances the PL emission lifetime as compared to less agglomerated samples.

Table 5 PL lifetime of the samples

Sample	Lifetime (μS)
S0	7.186 ± 0.132
S1	7.174 ± 0.099
S2	7.498 ± 0.075
S3	7.795 ± 0.150
S4	7.180 ± 0.139

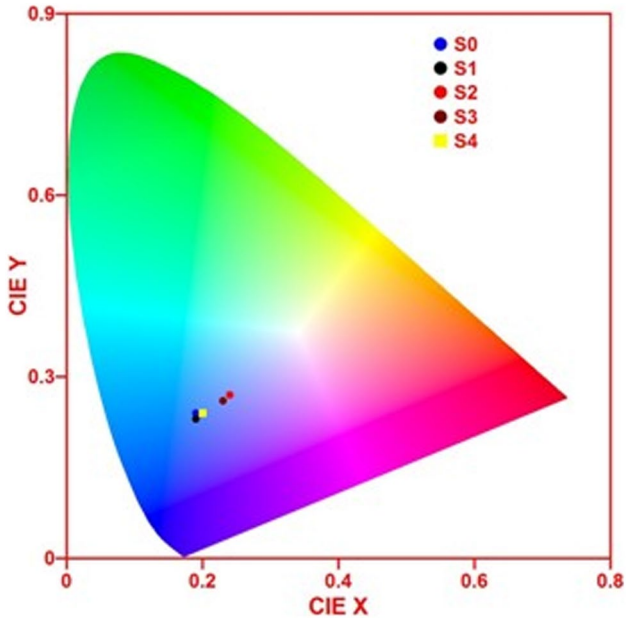

Fig. 13 CIE chromaticity coordinates of the $CoWO_4$ and $CoWO_4/PbWO_4$ nanocomposites

The CIE (Commission Internationale de I'Eclairage 1931) chromaticity coordinates of the samples S0, S1, S2, S3 and S4 measured to be (0.190, 0.240), (0.190, 0.230), (0.240, 0.270), (0.230, 0.260) and (0.200, 0.240) respectively are presented in Fig. 13. It indicates that all the CIE color coordinates are located in the blue region. Also due to higher PL intensities the positions of the coordinates for the highly agglomerated samples S2 and S3 are different than that of the other samples.

4 Conclusions

$CoWO_4$ and $CoWO_4/PbWO_4$ nanocomposites (crystallite size between 24 and 40 nm by Scherrer formula) were successfully prepared in an aqueous medium by simple co-precipitation method without using surfactant and

characterized. Crystallite size, band gap energy, PL intensity and lifetime were found to be controlled by Pb/Co atomic ratio. All the samples showed characteristic PL emission of $CoWO_4$. The highly agglomerated sample S3 was giving maximum PL emission which is approximately four times greater than that of S0 ($CoWO_4$) sample. This is attributed to the cluster-to-cluster maximum charge-transfer (CCCT) process between $[WO_4]^{2-}$ in $PbWO_4$ and $[WO_6]^{6-}$ in $CoWO_4$ complexes on the surface possibly due to interfacing of the $CoWO_4/PbWO_4$ nanocomposites because of high agglomeration. This lead to more number of recombinations of electron hole pairs in $CoWO_4$. Since luminescence is a surface property larger particle size may also contribute to the increase in the PL emission. This nanocomposite can be considered for producing blue component of emission for white LED.

Acknowledgements The authors are extremely thankful to Dr. Shyam Prasad and Mr. Areef A. Sardar of Geological Oceanography division, NIO, Goa for EDS measurements, Prof. K. R. Priolkar, Department of Physics, Goa University, Goa for helping to check the consistency of PL spectra with Cary eclipse fluorescence spectrometer and MRC, MNIT Jaipur, India for Zeta potential measurements. One of the authors M. Jeyakanthan is grateful to UGC, New Delhi, for providing BSR fellowship.

Compliance with ethical standards

Conflict of interest The authors declare that they have no conflict of interest.

References

1. F. Sun, X. Qiao, F. Tan, W. Wang, X. Qiu, One-step microwave synthesis of Ag/ZnO nanocomposites with enhanced photocatalytic performance. J. Mater. Sci. **47**, 7262 (2012)
2. C.S.S.R. Kumar, UV-VIS and photoluminescence spectroscopy for nanomaterials characterization, in *Optical properties of nanocomposites*, ed. by T Connor, M Zamkov (Springer, Berlin, 2013), pp. 485–522
3. Y.V.B. De Santana, J.E.C. Gomes, L. Matos, G.H. Cruvinel, A. Perrin, C. Perrin, J. Andres, V. Jose, E. Longo, Silver molybdate and silver tungstates nanocomposites with enhanced photoluminescence. Nanomater. Nanotechnol. **4**, 22 (2014)
4. J.M. Lin, C.L. Cheng, H.Y. Lin, Y.F. Chen, Giant enhancement of band edge emission in ZnO and SnO nanocomposites. Opt. Lett. **31**, 3173–3175 (2006)
5. X. Jiang, X. Zhao, L. Duan, H. Shen, H. Liu, T. Hou, F. Wang, Enhanced photoluminescence and photocatalytic activity of ZnO-$ZnWO_4$ nanocomposites synthesized by a precipitation method. Ceram. Int. **42**, 15160–15165 (2016)
6. Y. Guo, G. Zhang, H. Gana, Y. Zhang, Micro/nano-structured $CaWO_4/Bi_2WO_6$ composite: synthesis, characterization and photocatalytic properties for degradation of organic contaminants. Dalton Trans. **41**, 12697–12703 (2012)
7. D. He, L. Wang, D. Xu, J. Zhai, D. Wang, T. Xie, Investigation of photocatalytic activities over $Bi_2WO_6/ZnWO_4$ composite under UV light and its photoinduced charge transfer properties. ACS Appl. Mater. Interfaces **3**, 3167–3171 (2011)
8. V. Tucureanu, A. Matei, I. Mihalache, M. Danila, M. Popescu, B. Bita, Synthesis and characterization of YAG:Ce,Gd and YAG:Ce,Gd/PMMA nanocomposites for optoelectronic applications. J. Mater. Sci. **50**, 1883–1890 (2015)
9. M. Mai, C. Feldmann, Microemulsion-based synthesis and luminescence of nanoparticulate $CaWO_4$, $ZnWO_4$, $CaWO_4$:Tb, and $CaWO_4$:Eu. J. Mater. Sci. **47**, 1427–1435 (2012)
10. S.M.M. Zawawi, R. Yahya, A. Hassan, H.N.M.E. Mahmud, M.N. Daud, Structural and optical characterization of metal tungstates (MWO_4; M = Ni, Ba, Bi) synthesized by a sucrose-templated method. Chem. Cent. J. **7**, 80 (2013)
11. V. Pankratova, L. Grigorjevaa, D. Millersa, S. Chernova, A.S. Voloshinovskii, Luminescence center excited state absorption in tungstates. J. Lumin. **94**, 427–432 (2001)
12. F.A. Kroger, Fluorescence of tungstates and molybdates. Nature **159**, 674 (1947)
13. W. Qu, W. Wlodarski, J.U. Meyer, Comparative study on micromorphology and humidity sensitive properties of thin-film and thick-film humidity sensors based on semiconducting $MnWO_4$. Sens. Actuators B **64**, 76–82 (2000)
14. S.J. Naik, U. Subramanian, R.B. Tangsali, A.V. Salker, Optical absorption and photoluminescent studies of cerium-doped cobalt tungstate nanomaterials. J. Phys. D **44**, 115404–115410 (2011)
15. U. Subramanian, S.J. Naik, R.B. Tangsali, A.V. Salker, Upconversion luminescence of cerium doped $CoWO_4$ nanomaterials. J. Lumin. **134**, 464–468 (2013)
16. J.J.J. Joy, N.V. Jaya, Structural, magnetic and optical behavior of pristine and Yb doped $CoWO_4$ nanostructure. J. Mater. Sci. **24**, 1788–1795 (2013)
17. C. Zhang, D. Guo, C. Hu, Y. Chen, H. Liu, H. Zhang, X. Wang, Large-scale synthesis and photoluminescence of cobalt tungstate nanowires. Phys. Rev. B **87**, 035416 (2013)
18. H.Y. Lin, Y.Y. Chou, C.L. Cheng, Y.F. Chen, Giant enhancement of band edge emission based on ZnO/TiO_2 nanocomposites. Opt. Exp. **15**, 13833 (2007)
19. S. Patole, M. Islam, R.C. Aiyer, S. Mahamuni, Optical studies of ZnO/Ag nanojunctions. J. Mater. Sci. **41**, 5602–5607 (2006)
20. A. Kalinko, A. Kuzmin, Raman and photoluminescence spectroscopy of zinc tungstate powders. J. Lumin. **129**, 1144–1147 (2009)
21. F.A. Danevich, S. Henry, H. Kraus, R. McGowan, V.B. Mikhailik, O.G. Shkulkova, J. Telfer, Scintillation properties of pure and Cd-doped $ZnWO_4$ crystals. phys. stat. sol. (a) **205**, 335–339 (2008)
22. S. Chernov, L. Grigorjeva, D. Millers, A. Watterich, Luminescence spectra and decay kinetics in $ZnWO_4$ and $CdWO_4$ crystals. phys. stat. sol. (b) **241**, 1945–1948 (2004)
23. W. Wang, S. Lee, H. Piao, D. Choi, Y. Son, Growth mechanism and photoluminescence properties of controlled $PbWO_4$ micro- and mesocrystals obtained by the surfactant-assisted solvothermal method. CrystEngComm **17**, 6548–6554 (2015)
24. F. Lei, B. Yan, H. Chen, Q. Zhang, J.T. Zhao, Surfactant assisted hydrothermal synthesis, physical characterization and photoluminescence of $PbWO_4$. Cryst. Growth Des. **9**, 373–3736 (2009)
25. C. Zhang, J. Zhang, Y. Li, J. Zhao, W. Wei, R. Yao, G. Jia, S. Shen, Fabrication, characterization, and luminescence properties of highly uniform $PbWO_4:Ln^{3+}$ (Ln = Tb, Eu, Dy, and Sm) hierarchical microspheres. J. Alloys Compd. **698**, 33–38 (2017)
26. M. Jeyakanthan, U. Subramanian, R.B. Tangsali (2015) Effect of Pb^{2+} doping on the luminescence properties of $CoWO_4$ nano ceramics. Proceedings of the industrial applications of nanostructured materials, T.N., India, pp 193–196
27. L.S. Cavalcante, J.C. Sczancoski, V.C. Albarici, J.M.E. Matos, J.A. Varela, E. Long, Synthesis, characterization, structural refinement and optical absorption behavior of $PbWO_4$ powders. Mater. Sci. Eng. B **150**, 18–25 (2008)

28. V.D. Mote, Y. Purushotham, B.N. Dole, Williamson-Hall analysis in estimation of lattice strain in nanometer-sized ZnO particles. J. Theor. Appl. Phys. **6**, 6 (2012)
29. Z.F. Liang, M.Y. Shuang, Influence of europium doping amount on properties of antimony doped tin oxide. Res. J. Appl. Sci. Eng. Technol. **6**, 2644–2648 (2013)
30. L.G. Qiang, G. Lian, L. Wei-Ling, H. Dong-Sheng, Relation between ζ potential and dispersity in the preparation process of nano-scale ZnO. J. Inorg. Mater. **14**, 813–817 (1999)
31. G.M. Clark, W.P. Doyle, Infra-red spectra of anhydrous molybdates and tungstates. Spectrochim. Acta **22**, 1441 (1996)
32. D. Sun, H.J. Sue, N. Miyatake, Optical properties of ZnO quantum dots in epoxy with controlled dispersion. J. Phys. Chem. C **112**, 16002–16010 (2008)
33. L. Li, J. Liu, Y. Su, G. Li, X. Chen, X. Qiu, T. Yan, Surface doping for photocatalytic purposes: relations between particle size, surface modifications and photoactivity of SnO_2: Zn^{2+} nanocrystals. J. Nanotechnol. **20**, 155706 (2009)
34. U. Ozgur, Y.I. Alivov, C. Liu, A. Teke, M.A. Reshchikov, S. Dogan, V. Avrutin, S.J. Cho, H. Morkocd, A comprehensive review of ZnO materials and devices. J. Appl. Phys. **200598**, 041301 (2005)
35. Y. Su, B. Zhu, K. Guan, S. Gao, L. Lv, C. Du, L. Peng, L. Hou, X. Wang, Particle size and structural control of $ZnWO_4$ nanocrystals via Sn^{2+} doping for tunable optical and visible photocatalytic properties. J. Phys. Chem. C **116**, 18508–18517 (2012)
36. L.S. Cavalcante, V.M. Longo, J.C. Sczancoski, M.A.P. Almeida, A.A. Batista, J.A. Varela, M.O. Orlandi, E. Longo, M.S. Li, Electronic structure, growth mechanism and photoluminescence of $CaWO_4$ crystals. Cryst. Eng. Commun. **14**, 853–868 (2012)
37. H. Huang, S. Wang, N. Tian, Y. Zhang, A one-step hydrothermal preparation strategy for layered $BiIO_4/Bi_2WO_6$ heterojunctions with enhanced visible light photocatalytic activities. RSC Adv. **4**, 5661 (2014)